MICROCOPY RESOLUTION TEST CHART

NATIONAL BUREAU OF STANDARDS-1963

Begin text of second and

2-D Simulations for Accurate Extraction of the Specific Contact Resistivity from Contact Resistance Data

W. M. Loh, S. E. Swirhun, T. A. Schreyer,
R. M. Swanson, and K. C. Saraswat

Center for Integrated Systems
Stanford University, Stanford , California 94305.

ABSTRACT

This paper presents a unified approach for the accurate extraction of specific contact resistivity (ρ_c) for ohmic contacts. Using 2-D simulations, which account for the current flow, or crowding around the contact window, we have analysed the resistance data obtained from the Cross Bridge Kelvin Resistor, the Contact End Resistor, and the Transmission Line Tap Resistor. For each particular structure, a universal set of curves is derived that allows accurate determination of ρ_c, given the geometry of the structure. The values obtained for ρ_c are independant of the test structure type, its geometry and the contact area. The data suggests that in the past researchers have overestimated ρ_c, and that contact resistance will not limit device performance even with submicron design rules.

INTRODUCTION

As MOS technology scales down into the submicron regime, it has been believed that the series resistances contributed by the source/drain contacts increase much more rapidly than the other resistance components [1]. This is because the contact resistance's scaling approaches λ^{-2} for small contacts [2], where λ is the minimum feature size. To determine if contact resistance is a limiting factor in the next generation ULSI, it is paramount to obtain accurate values of the specific contact resistivity ρ_c, the physical parameter that governs the interfacial contact resistance between the contact material and the diffusion. There are three test structures commonly used to extract ρ_c: the Cross Bridge Kelvin Resistor (CBKR) [3], the Contact End Resistor (CER) [4], and the Transmission Line Tap Resistor (TLTR) [5] as shown in Fig. 1. In all of these structures, a current is sourced from the diffusion level up into the metal level via the contact window and a voltage is measured between the two levels using two other terminals. The contact resistance for each structure is simply this voltage divided by the source current. It is important to realize that each device measures the voltage at a different position along the contact, hence the resistance values measured are different, and must be clearly defined and distinguished from one another. In this paper, they are referred to as R_k (Kelvin), R_e (end), and R_f (front) for the CBKR, CER, and TLTR respectively.

There are two problems which make it very difficult to extract ρ_c accurately from the contact resistance measurements, using the present theoretical 1-D equations (given in Fig. 1). The first problem is that when these three structures are used to measure similar contacts, the results often yield conflicting estimates of ρ_c. The second problem is that when contact resistance is plotted against area, a sublinear behavior is observed for CBKR, instead of the expected inverse linear behavior [6-7]. The extracted values of ρ_c not only appear to be area dependent, but also a function of diffusion sheet resistance R, even though the active surface dopant concentrations are the same. This is a serious problem since the variations are often more than an order of magnitude. Previous work [8-12] has attributed these phenomena to two-dimensional (2-D) current flow, or crowding, in the diffusion-tap area around the contact window. Those analyses partially explain these phenomena but do not explain how to overcome the problem. Hence, there is a need for deeper understanding and unified methodology. In this paper, a unified 2-D model is presented which circumvents these shortcomings and provides an

explanation of the two phenomena. The novel extraction method derived from the unified 2-D model provides values of ρ_c which are accurate and self-consistent independent of geometry and test structure types.

TWO-DIMENSIONAL MODEL

For relatively shallow junctions, a diffusion can be characterized completely by its sheet resistance. We shall concentrate here on semiconductor to metal contacts. Since the metal sheet resistance is much lower than diffusion sheet resistance, metal is considered to be an equipotential plane. Therefore the current flow in the diffusion-contact system can be described entirely by the potential in the diffusion "sheet" which is governed by the Helmholtz equation:

$$\frac{\partial^2 V}{\partial x^2} + \frac{\partial^2 V}{\partial y^2} = \frac{V}{l_t^2} \tag{1}$$

in the diffusion area directly beneath the contact and by the Laplace equation:

$$\frac{\partial^2 V}{\partial x^2} + \frac{\partial^2 V}{\partial y^2} = 0 \tag{2}$$

elsewhere. The transfer length l_t is defined as (ρ_c / R_s)$^{1/2}$; a length that characterizes how far the current travels in the diffusion area beneath the contact before passing into the metal level. For all three test structures, a ratio between a measured potential (V^*) and the source current (I) gives a resistance R^*. The resistance ratio R^* / R_s can be expressed as a function of l_t :

$$\frac{R^*}{R_s}(l_t) = \frac{V^*}{\int_{d_1} \frac{\partial V}{\partial x} dy} \tag{3}$$

where d_1 is a line perpendicular to the current flow. Note that the denominator represents the total current flowing into the contact window divided by the sheet resistance. Using numerical techniques [13], we have solved equations (1) and (2) to find $V(x,y,l_t)$ for a wide ranging set of test structure geometries. Then R^* / R_s is evaluated via the solution of (3). By comparing the experimentally measured resistance ratio to the one generated by the 2-D simulations using l_t as a parameter, a unique value of l_t can be extracted and the accurate value of ρ_c obtained for each test structure. The use of l_t allows contact resistivity and sheet resistance to be lumped together as a single parameter, which reduces the simulation task to one independent parameter for a specified test structure geometry. The problem is further reduced by considering only the ratio of measured resistance to sheet resistance.

EXTRACTION OF ρ_c USING 2-D MODEL

In Fig. 2, the ratio of the Kelvin contact resistance R_k to R_s is shown as a function of contact area for the CBKR structure. The overlap δ, which is the difference between the contact size and diffusion width is maintained at 2.5 μm. The diagram shows the sublinear behavior in the experimental data and an accurate prediction of it by the 2-D model. The 1-D model predicts only a linear behavior ($R_k = \rho_c / l^2$) because it is unable to account for current crowding effects. The diagram shows that there is a large deviation from the 1-D model as l_t is decreased. This is due to a parasitic component added to the ideal value of ρ_c / l^2 due to

ALL MATERIAL IN THIS SPACE WILL BE DELETED

current crowding effects. This is more pronounced for large contact areas and small values of l_t. For low ρ_c and high R_n serious crowding occurs and 2-D simulations are required to accurately model the behavior of the data as shown. Good agreement between simulations and measured values implies accurate extraction of different l_t for the metal (W, Al, PtSi) to N^+/P^+ (B, P, As) diffusions. The results are summarized in Table 1.

In Fig. 3 the 2-D model is compared to the 1-D model for the contact end resistor where δ is 2.5 μm. The 2-D model shows that the 1-D model severely underestimates this resistance. This is due to current flowing around the overlap area and into the contact end. The error can be as high as several orders of magnitude for low values of l_t [14]. This shows that when the 1-D equation for the CER is used to extract low ρ_c values, the true ρ_c is overestimated by at least an order of magnitude.

To study the effect of the current flowing in the overlap region, CER test structures were fabricated in which the diffusion-tap width w was varied while the contact size is kept constant at 5 μm. The data and simulations are shown in Fig.4. For curve 1, the value of R_s is independant of w, implying that the 1-D model is sufficient for this high value of ρ_c. But curves 2 and 3 show a strong dependance on w, which cannot be accounted for by the 1-D model. Once more, the 2-D predictions track the measured data accurately as shown. For PtSi to P diffusion (curve 2), the extracted value of ρ_c is 5 Ω μm^2, which agrees with the CBKR value obtained earlier on the same wafer. We have also extracted an identical value of ρ_c with the TLTR structure, and it is much lower than previously reported values.

The third structure to be examined, the TLTR, measures the "front" resistance indirectly. The "front" potential-- the contact potential near the leading edge of the contact is larger than the potential on the side as sensed by the CBKR and much larger than the contact end potential in the CER case. Therefore, the 2-D crowding effect has much less impact on the TLTR than the other two structures. In fact, it is possible to design a TLTR which is essentially 1-D by making the contact width much larger than its length. The effect of 2-D crowding on the front resistance of square contacts is shown in Fig. 5. For these contacts, the 1-D model is off by less than an order of magnitude even for very low values of l_n signifying that the current crowding effect is not serious for this structure. Unfortunately, the TLTR structure introduces another source of error because it can only measure the front resistance indirectly. The measured resistance is the sum of the front resistance and series diffusion sheet resistance, and these two components must be isolated by extrapolation techniques.

The graphs displayed to this point are useful for extracting accurate values of ρ_c. By making several devices with different geometries, the R_c / R_s ratios can be plotted on the appropriate curve, and ρ_c can be extracted. The consistency of the extracted ρ_c values can and should be used as a gauge to judge the validity of the experiment. So far, only one geometric variable can be varied at a time in each study. In order to make possible the extraction of ρ_c for a very wide range of design rules, this constraint is removed in the next section.

GENERALIZED EXTRACTIONS

If the dimensions of the test structures are normalized by dividing each by a characteristic length L, then equations (1) and (2) will become:

$$\frac{\partial^2 V}{\partial (\frac{x}{L})^2} + \frac{\partial^2 V}{\partial (\frac{y}{L})^2} = \frac{V}{(\frac{l_t}{L})^2} \tag{4}$$

$$\frac{\partial^2 V}{\partial (\frac{x}{L})^2} + \frac{\partial^2 V}{\partial (\frac{y}{L})^2} = 0 \tag{5}$$

The general resistance ratio in equation (3) will still retain the same form but the independent parameter is now $\frac{l_t}{L}$:

$$\frac{R^*}{R_s} = \frac{R^*}{R_s} (\frac{l_t}{L}) \tag{6}$$

This shows that there is a simple scaling law which may be used to normalize all of the above simulations:

$$\frac{R^*}{R_s} (l, w, l_t) = \frac{R^*}{R_s} (\frac{l}{L}, \frac{w}{L}, \frac{l_t}{L}) \tag{7}$$

where l and w are the contact length and diffusion width, respectively. The characteristic length L can be any one of the geometric variables used to define the dimensions of the contact structures. A convenient L would be the overlap δ because it is not varied over a large range.

This scaling law allows all of the previous simulations to be normalized, providing three sets of generalized curves. (It is still necessary to differentiate between front, end, and Kelvin resistance.) These curves eliminate the need for further 2-D simulations since all practical dimensions of contacts and diffusions, and all contact-resistivites and diffusion sheet resistances are contained in one diagram. The application is demonstrated in Fig. 6. The resistance ratio is plotted against the dimensionless ratio l / δ with parameter l_t / δ. When $l_t \gg \delta$, the behavior is essentially 1-D and the curves are straight. But as l_t decreases below δ, the 2-D current crowding effect becomes significant, especially in the cases of large contacts. The extraction accuracy in this case is rather low as is shown in the close packing of the curves in this regime of low ρ_c. As contact size shrinks, the curves spread out more evenly and the extraction accuracy is improved. Also note that the effect of reduced δ results in improved accuracy.

The generality of the universal curves is demonstrated in Fig. 7. The 2-D simulations and experimental data of two sets of CBKR's fabricated on the same wafer with only a difference in δ (1.25 μm, 2.5 μm) are shown. The extracted l_t is the same (0.5 μm), indicating once more that ρ_c is independent of geometry of test structure.

A similar set of universal curves for CER is shown in Fig. 8. The main difference is that the values of the contact resistance are lower than those of CBKR. This requires measurement of significantly smaller voltages if current densities are kept the same. Furthermore, the resistance ratio decreases rapidly as δ increases and thus the sensitivity of the variaiton in δ is high. This is because the end contact potential is a strong function of l_t / l.

The TLTR is far less sensitive to δ because it detects the front contact potential. Although the solid lines in Fig. 9 indicate that the TLTR has slightly less geometric sensitivities than the CBKR, there is another source of error caused by the indirect measurement method in extrapolation of the contact resistance from the resistance between two close contacts as shown in Fig. 1. When R_s is large, the extrapolation becomes quite difficult and sensitive to small variations in the separation distance between the contacts. But the next example will demonstrate that with careful electrical and optical measurements the universal extraction curves yield an accurate value of ρ_c. The R_f / R_s values of the TLTR devices on a single wafer were measured using separation distances and overlaps measured by optical and electrical techniques. The data was then plotted as symbols along with the universal curves in Fig. 9. At first glance, the data points appear scattered and poorly fitted to any single curve. But by estimating the value of l_t / δ and then multiplying this by the measured value of δ, these data points all give ρ_c values within 20% of each other. This agreement further strengthens the validity of the generalized method. Using this technique we have measured ρ_c for PtSi, W and Al contacts to N^+ and P^+ Si for a wide range of dopant concentration. The datailed results will be presented.

CONCLUSIONS

We have developed a technique which allows accurate and unambiguous determination of contact resistivity even at low values. In the examples illustrated, this technique repeatedly yields the same value of ρ_c for a wide variety of contact dimensions and test structures on a single wafer. The results of the 2-D model are presented in a universal form so that they may be used for extractions without performing any additional simulations. The new model points out that the 1-D model seriously overestimates the specific contact resistance due to 2-D current crowding in the overlap region. This implies that most reported values of ρ_c
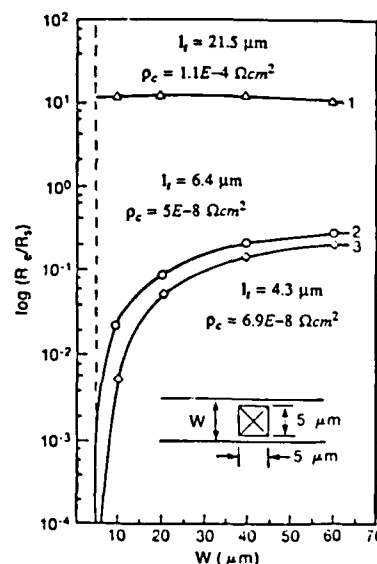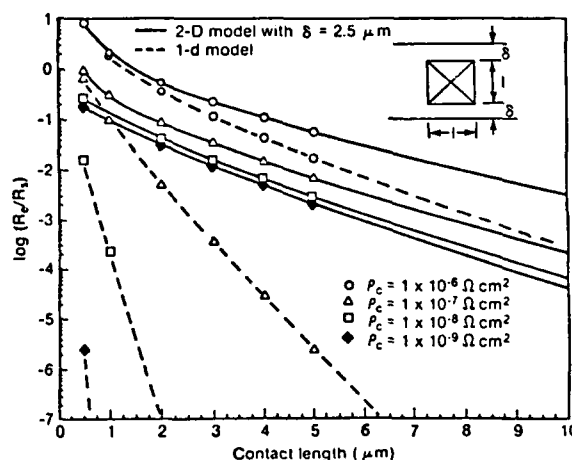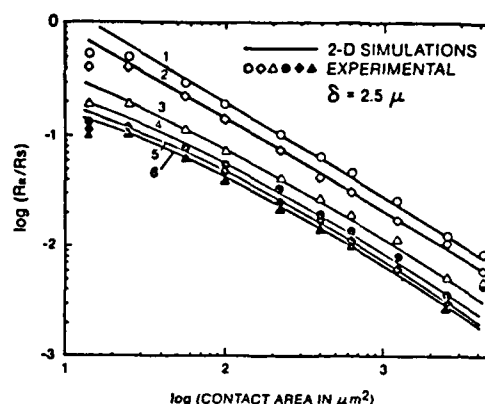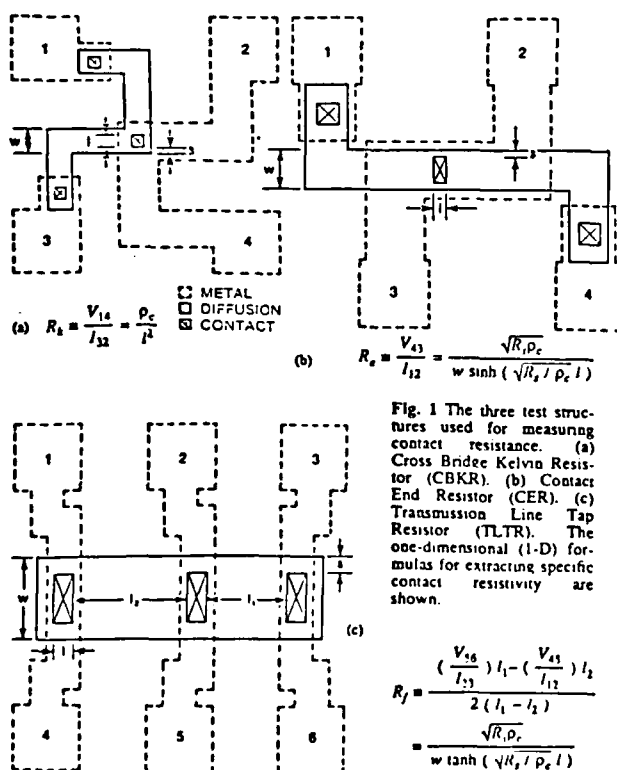
extracted by using the 1-D method are overestimated, and that ρ_c will not be a limiting factor for ULSI.

ACKNOWLEDGEMENTS

REFERENCES

[1] W. Fichtner, IEDM 82 Tech. Dig., SF, p. 638

[2] R. H. Dennard et al., IEEE JSSC vol. 9-5, p. 256, Oct. 74.

[3] S. J. Proctor et al., IEEE TED 30-11, p. 1535, Nov. 83.

[4] J. Chern et al., IEEE EDL-5, p. 178, May 84.

[5] H. H. Berger, ECS Journal 119-4, p. 507, Apr. 72.

[6] R. L. Maddox, TED 32-3, p. 682, Mar. 85.

[7] J. M. Ford, IEEE TED 32-4, p. 8402, Apr. 85.

[8] M. Finetti et al., IEEE EDL 5-12, p. 524, Dec. 84.

[9] W. M. Loh et al., IEEE EDL 6-3, p. 105, Mar. 85.

[10] M. Finetti et al., IEEE Electron EDL 6-4, p. 184, Apr. 85.

[11] N. P. Armstrong et al., VLSI Multilevel Interconnection Conference, Santa Clara, p. 389, June 85.

[12] W. M. Loh et al., IEEE EDL 6-9, p. 441, Sept. 85.

[13] M. Pinto et al., Stanford Elec. Lab Tech. Rep., Oct. 84.

[14] S. E. Swirhun et al., submitted to EDL.

Fig. 2 The ratio of Kelvin contact resistance to diffusion sheet resistance plotted as a function of contact area for different transfer length l, for CBKR with overlap being 2.5 μm. Symbols denote measured data, solid lines are simulations.

Fig. 3 Simulated end contact resistance for the CER structure with square contact holes. Lines and symbols both denote simulations only. Solid lines are the 2-D model; dashed lines are the 1-D model.

(a) $R_k = \dfrac{V_{14}}{I_{32}} = \dfrac{\rho_c}{l^4}$

(b) $R_e = \dfrac{V_{43}}{I_{12}} = \dfrac{\sqrt{R_s\rho_c}}{w\sinh(\sqrt{R_s/\rho_c}\, l)}$

Fig. 1 The three test structures used for measuring contact resistance. (a) Cross Bridge Kelvin Resistor (CBKR). (b) Contact End Resistor (CER). (c) Transmission Line Tap Resistor (TLTR). The one-dimensional (1-D) formulas for extracting specific contact resistivity are shown.

(c)

$R_f = \dfrac{(\dfrac{V_{56}}{I_{23}})\,l_1 - (\dfrac{V_{43}}{I_{12}})\,l_2}{2(l_1 - l_2)}$

$= \dfrac{\sqrt{R_s\rho_c}}{w\tanh(\sqrt{R_s/\rho_c}\, l)}$

Fig. 4 End resistance as a function of diffusion width for constant contact size of 5 μm. Symbols denote actual measurements; lines are 2-D simulations.

Table 1 Summary of extraction results for the data shown in Fig. 2.

Num.	Metal	Dopant	R_s ($\Omega/sq.$)	l_t (μm)	ρ_c ($\Omega \mu m^2$)
1	W	As	422	3.5	3500
2	W	B	71.4	2.75	540
3	Al	B	12.4	1.4	24.3
4	Al	B	71.1	0.9	57.6
5	PtSi	P	12.1	0.65	5.11
6	W	As	44.4	0.5	11.1

Fig. 7 Illustration of the use of the CBKR universal curve to extract l_t from structures with different overlap δ on the same wafer. $l_t = 0.5 \mu m$ for all points.

Fig. 5 Simulated front contact resistance for the TLTR structure with square contact holes. Lines and symbols both denote simulations only. Solid lines are the 2-D model; dashed lines are the 1-D model.

Fig.8 Generalized universal curves for the CER. Curves show l_t / δ approximately in octave steps.

Fig. 6 Generalized universal curves for the CBKR. Curves show l_t / δ in octave steps.

Fig.9 Generalized universal curves for the TLTR. Curves show l_t / δ in approximate octave steps. Symbols show data from devices on the same wafer which have a variety of overlap sizes.

END

DTIC

8-86